High performance encapsulation of transparent conductive polymers by spatial atomic layer deposition

Amélie Schultheiss, Abderrahime Sekkat, Viet Huong Nguyen, Alexandre Carella, Anass Benayad, Amélie Revaux, Renaud Demadrille, David Muñoz-Rojas, Jean-Pierre Simonato

Version of Record: https://www.sciencedirect.com/science/article/pii/S0379677921003015
Manuscript_d4807b344e9d4de3c208173b49abe74e

High Performance Encapsulation of Transparent Conductive Polymers by Spatial Atomic Layer Deposition

Amélie Schultheiss,[1,⊥] Abderrahime Sekkat,[2,⊥] Viet Huong Nguyen,[4] Alexandre Carella,[1] Anass Benayad,[1] Amélie Revaux,[1] Renaud Demadrille,[3] David Muñoz-Rojas, [2,*] Jean-Pierre Simonato,[1,*]*

[1] Univ. Grenoble Alpes, CEA, LITEN, DTNM, F-38000 Grenoble, France

[2] Univ. Grenoble Alpes, CNRS, Grenoble INP, LMGP, F-38000 Grenoble, France

[3] Univ. Grenoble Alpes, CNRS, CEA, INAC, SyMMES, 17 rue des martyrs, 38000 Grenoble,

[4] Faculty of Materials Science and Engineering, Phenikaa University, Hanoi 12116, Vietnam

[⊥] These authors contributed equally to this work

***Corresponding authors**

Email addresses: amelie.schultheiss@gmail.com, david.munoz-rojas@grenoble-inp.fr, jean-pierre.simonato@cea.fr

Abstract

Poly(3,4-ethylenedioxythiophene) (PEDOT) is a transparent conductive polymer widely used in flexible photonic and optoelectronic devices because of its excellent electrical and optical properties. However, its current range of applications is limited by its poor stability under high humidity and solar radiations. Encapsulation is an attractive solution to this problem and the development of a low-temperature and scalable deposition method is highly desirable. In this study, we report the use of spatial atomic layer deposition (SALD) to deposit ultrathin layers of ZnO, TiO_2, and Al_2O_3. These nanolayers maintain the electrical performance of the conductive polymer and its high optical transmittance. The use of SALD ensures low-cost and flexible processing with pinhole-free high-quality coatings at atmospheric pressure and high-throughput. The present study is the first to investigate the effect of various multilayer metal oxide encapsulations on the long-term stability of PEDOT-based transparent conductive materials under solar radiations. We demonstrate finally that bilayer TiO_2/Al_2O_3 and TiO_2/ZnO coatings preserve the optoelectronic properties of three different PEDOT-based films, namely PEDOT:OTf (OTf = triflate), PEDOT:Sulf (Sulf = sulfate)and PEDOT:PSS (PSS = PolyStyreneSulfonate) films.

Keywords: poly(3,4-ethylenedioxythiophene), PEDOT, SALD, aging, encapsulation, degradation

1. INTRODUCTION

Conductive polymers have a wide range of applications including in organic electronics, photovoltaics, energy storage, and smart biomaterial devices.[1–6] In electronic and optoelectronic devices, poly(3,4-ethylenedioxythipohene) (PEDOT), one of the most promising conductive polymers, balances conductivity and transparency just as well as ITO (indium tin oxide), with the additional benefits of scalable processing, low cost, and flexibility.[7–15] However, one of the main drawbacks of this material, and of organic materials in general, is their poor stability under environmental stress (high humidity, solar radiations).[16] The development of techniques to improve the stability of polymeric conductive films is therefore crucial. For PEDOT, several encapsulation films and methods have been evaluated in this context. For example, Chen et al. extended the half-life of PEDOT more than 10-fold by capping it with poly(divinylbenzne-co-maleic anhydride, PDVB-MA),[17] although the latter did still degrade over time. Spatial atomic layer deposition (SALD), an alternative to conventional ALD, has shown promise in device integration since it was first published in 2008.[18] In this straightforward and scalable method, reactive precursors are separated in space rather than in time, allowing metal oxide films to be deposited under ambient conditions at remarkably high rates.[19–24]

Metal oxide films are efficient encapsulating coatings since they protect the underlying layer from UV radiations and act as a barrier against water and oxygen. Aluminum oxide (Al_2O_3) has

interesting gas diffusion barrier properties,[25],[26] while zinc oxide and titanium dioxide (ZnO and TiO_2) are commonly used as UV filters.[27],[28] Gas barrier oxides are useful for sunlight protection because materials are generally sensitive to the combination of radiation (mainly UV) and water vapor or oxygen.[16] For example, metal oxide films have successfully been used to improve the stability of silver and copper nanowire networks under harsh conditions.[29],[30] The effects of metal oxide coatings on organic materials have not been so well studied because it is difficult to deposit a protective layer uniformly and conformally on ultrathin polymeric substrates without damaging them.[31–33] Further requirements for the deposition technique are that it should be cost-effective, high-throughput, low-temperature, vacuum-free and compatible with roll-to-roll processing while still yielding high-quality, pinhole-free coatings. SALD thus appears as an ideal technique to apply protective oxide coatings to organic devices. Indeed, Mutee Ur Rehman et al. enhanced the lifetime of PEDOT:PSS in an organic sensor thanks to an Al_2O_3 layer, applied by SALD.[34] Similarly, Choi et al. and Maydannik et al. used an Al_2O_3 layer as a gas barrier to improve the water vapor transmission rate (WVTR) of organic displays.[35,36]

In this study, we evaluated the performance of several multilayer structures as encapsulation layers for PEDOT:triflate (PEDOT:OTf, see Figure S1), PEDOT:sulfate/hydrogen sulfate (PEDOT:Sulf, the sulfuric treated version of PEDOT:OTf, with higher conductivity but lower stability) and PEDOT:polystyrene sulfonate, post-treated with ethylene glycol (PEDOT:PSS-EG), as reference product. We focused on their stability under solar radiations because of the widespread use of PEDOT in photovoltaics,[37–40] and because these materials are known to be particularly susceptible to radiation damage (mainly because of chain scission, degradation of counter-anions and crystallinity).[41] Given their intended use in optoelectronic devices, the PEDOT films were prepared in thin layers of around 30 nm for at least 85% total transmittance

(knowing that the haze factor of these materials is less than 1%), and a sheet resistance of around 150 $\Omega.sq^{-1}$. The polymer films were protected with layers of Al_2O_3, ZnO, and/or TiO_2.[42] The novelty of this work lies in the deposition of metal oxides on organic layers under ambient conditions (temperatures below 200°C, without need of vacuum chamber), using SALD. Moreover, we used the superposition of several (two or three) oxide layers to combine their advantages.[43] The effects of the precursors on the polymeric films, notably on the doping level, were studied by UV-Vis-NIR spectroscopy and soft and hard X-ray photoelectron spectroscopy (S-XPS and HAXPES).The oxide layers were then tested alone and in combination to encapsulate the different PEDOT films under sunlight radiations.

2. EXPERIMENTAL SECTION

2.1. Materials

3,4-ethylenedioxythiophene (EDOT), N-methyl-2-pyrrolidone (NMP), isopropanol (IPA), iron(III) trifluoromethanesulfonate ($Fe(OTf)_3$), polyethylene glycol − polypropylene glycol − polyethylene glycol (PEG–PPG–PEG) Mw = 5800 g/mol and ethylene glycol (EG) were obtained from Sigma-Aldrich. Anhydrous ethanol was purchased from CARLO ERBA Reagents. PEDOT:PSS CLEVIOS TM PH1000 was purchased from Heraeus. Glass substrates (7.5 × 2.5 cm^2, 0.96 to 1.06 mm thick) were purchased from Corning.

2.2. PEDOT deposition

PEDOT:OTf and PEDOT:Sulf films were prepared as follows: $Fe(OTf)_3$ was dissolved at 0.126 mg/mL in a solution containing 72.25 wt % of ethanol, 20.00 wt % of PEG–PPG–PEG, and 7.75 wt % of NMP. The solution was sonicated for 2 h, then 0.25 mL of this solution was mixed with 5 µL of EDOT before being spin-coated onto the substrate (Glass or PEN), at 4500

rpm for 30 s. The resulting films were heated on a hot plate at 70°C before being rinsed with ethanol and dried again at 70 °C, yielding to PEDOT:OTf. To prepare PEDOT:Sulf, PEDOT:OTf film was dipped in 0.1 M sulfuric acid for 30 min before being dried on a hot plate at 120 °C for 30 min, to allow substitution of a large part of the triflate anions by sulfate or hydrogen sulfate groups.

PEDOT:PSS-EG films were prepared as follows: commercial PEDOT:PSS (Clevios PH1000) was mixed with IPA (50:50 vol). The surface was covered by the solution and spin-coated at 1000 rpm for 1 min, with an acceleration of 500 rpm/s. The film was heated at 120 °C for 10 min on a hot plate, then dipped in EG for 30 min before being rinsed in ethanol and dried once more on a hot plate at 120 °C for 30 min.

To measure the electrical resistance of the films, gold electrodes were deposited at the edges of square samples (2.5×2.5 cm²) so that the resistance values obtained were equivalent to the sheet resistance of the film in $\Omega.sq^{-1}$.

2.3. SALD of metal oxide layers

The TiO_2 thin films were deposited using a custom-built SALD system.[44] Titanium tetrachloride ($TiCl_4$) and water vapor were carried to the manifold head at flow rates of 10 sccm for $TiCl_4$ and 100 sccm of H_2O, diluted in 25 and 100 sccm of N_2, respectively. Nitrogen was used as an inert gas barrier with a total flow rate of 450 sccm. The temperature of the substrate was maintained at 150 °C. The distance between the substrate and the SALD injection head was approximately 150 µm with a scanning speed of 10 cm/s. The precursor for the Al_2O_3 layers was trimethylaluminium (TMA), which was carried at 15 sccm with 150 sccm H_2O, diluted in 235 and 225 sccm of N_2, respectively. The N_2 barrier total flow was 750 sccm. Different deposition

temperatures (100, 150 and 200 °C) were tested and the number of deposition cycles was varied from 10 to 90, to adjust the thickness of the films from 9 to 81 nm. Diethylzinc precursor $(C_2H_5)_2Zn$ (DEZ) was used to deposit ZnO, using a flor of 30 sccm with 150 sccm of H_2O, respectively diluted in 270 and 300 sccm of N_2. The N_2 barrier total flow was 900 sccm. The deposition temperature was varied between 50 °C and 200 °C and the number of deposition cycles was varied from 10 to 60 to obtain thicknesses between 5 and 55 nm.

2.4. Characterizations

Soft-X-ray photoelectron spectra were recorded using a Versaprobe II ULVAC-PHI spectrometer. A monochromatic beam (X-ray source, Al Kα, 1486.6 eV; diameter, 100 μm; power, 50 W) was focused on the surface of the samples. High-resolution spectral analyses were performed using a pass energy of 23 eV, corresponding to a resolution of 0.5 eV. All XPS measurements were carried out in an ultrahigh vacuum chamber ($7x10^{-10}$ mbar). The spectrometer was calibrated using the photoemission lines of gold (Au 4f7/2 = 84.0 eV, with reference to the Fermi level). Dual charge neutralization was used to avoid any eventual charging effect induced at the surface of the samples. All XPS spectra binding energies were corrected using the C1s line of carbon sp^3 at 285.0 eV. As the S-XPS is a surface analysis technique (depth analyses of 5 nm). To probe deeper (~20 nm) into the films, HAXPES data were recorded on a PHI-Quantes spectrometer. A monochromatic beam (X-ray source, Cr Kα, 5414.9 eV) of 100 μm of diameter and 50 W was used. High-resolution spectral analyses were performed using a pass energy of 69 eV, corresponding to a resolution of 0.8 eV. Depth profiling analyses were performed using an argon Gas Cluster Ion Beam (GCIB), at 8 eV/atom with a current density of 5

nA/mm^2, which was used instead of a conventional Ar ion beam to avoid chemical destruction during depth profiling.

Resistances were measured at room temperature (T= 20-25°C, for relative humidity RH≈ 40%) with a two-probe ISO-TECH IDM19 multimeter. UV-vis-NIR spectra were recorded on a Varian Cary 5000 device. Sun aging experiments were performed using an ABET Sun 3000 solar simulator calibrated at 1000 W/m².

3. RESULTS AND DISCUSSION

We first studied the effects of SALD on the electrical performance of PEDOT:OTf. ZnO, Al_2O_3 and TiO_2 where thus deposited at an initial temperature of 150 °C (due to the organic nature of PEDOT) and 10 to 90 deposition cycles (corresponding to layer thicknesses of 9–81 nm), to preserve high optical transparency. Figure 1a shows how the resistance of the polymer–oxide systems varied over time under 1 sun (1000 W/m²) illumination, using the measurement setup shown in Figure 1b.

For Al_2O_3, the initial R/R_0 ratio ranged from 1.81 after 10 SALD cycles to 2.46 after 90 (Figure S2a), possibly because of the reducing effect of the trimethylaluminum (TMA) precursor.[45] Increasing the thickness of the alumina layer does not drastically increase the resistance of the composite, presumably because reduction only occurs at the interface and also acts as a protective gas barrier. The overall transmittance does not decreases linearly as the thickness increases because the change in density of the film affects its refractive index. Overall,

the protective effect of alumina does not compensate for the initial deterioration in electrical properties.

With ZnO, while the increase in resistance for the thinnest deposited layer was similar to that observed for Al_2O_3, R/R_0 varied substantially with the thickness of the deposited layer (sevenfold higher when 30 deposition cycles were used instead of 10, as displayed in Figure S2b). The diethylzinc precursor ($(C_2H_5)_2Zn$, DEZ) is reactive,[46] as is TMA, but contrary to Al_2O_3, ZnO is less efficient as a gas barrier (being mostly a UV filter), and therefore does not afford the same protection that Al_2O_3 does as the number of deposition cycles is increased. To reduce the reactivity of DEZ on PEDOT, ZnO was also deposited at a lower temperature (50 °C), but the resulting coatings provided less protection than did the thinnest layer deposited at 150 °C. At 50 °C indeed, the deposited layers are probably not dense or crystalline enough to provide effective UV protection.[47,48] Figure 1a shows that aside from the initial alteration of the PEDOT:OTf due to the deposition process, the samples protected by a thin layer of ZnO (10 SALD cycles at 150 °C) remained remarkably stable, with a R/R_0 slope of just 0.0005 h^{-1} compared with 0.0096 h^{-1} for the unprotected sample, equating to a 19-fold decrease in the degradation rate.

The precursor for TiO_2, $TiCl_4$ leads to the formation of HCl as by-product during deposition. Acids have been shown to increase the electrical conductivity of PEDOT,[49,50] even in the gas phase.[51] Here, TiO_2 deposition was indeed observed to slightly increase the electrical conductivity of PEDOT:OTf, even for the thickest layers (63 nm, 90 SALD cycles, Figure S2c). The HCl(g) by-product presumably leads to the release of chloride counter ions which have a doping effect on the PEDOT. Surprisingly however given the moderate gas barrier and UV filter properties of TiO_2, these layers did not reduce the degradation rate of PEDOT:OTf under solar radiations (Figure 1a), indicating that TiO_2 is not effective in this context when used alone.

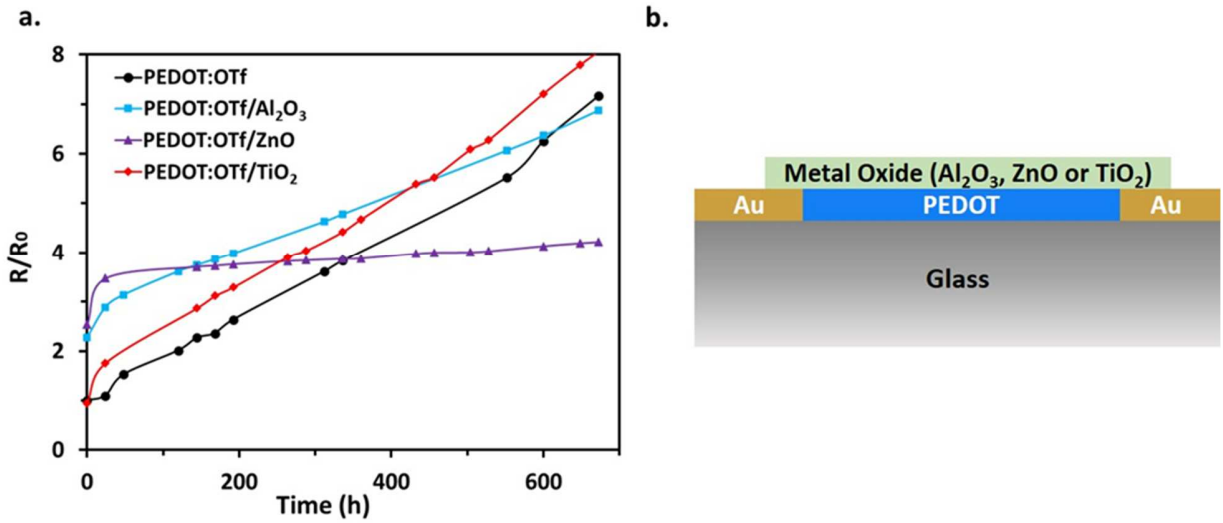

Figure 1. (a) Time evolution of the resistance of different PEDOT:OTf systems under 1 sun illumination (1000 W/m²): non-encapsulated PEDOT:OTf (black curve), PEDOT:OTf encapsulated with Al_2O_3 (10 SALD cycles at 150°C, blue curve), ZnO (10 SALD cycles at 150°C, purple curve) or TiO_2 (30 SALD cycles at 150°C, red curve). R_0 corresponds to the resistance measured before oxide deposition and irradiation. (b) Schematic representation of the encapsulated system and experimental setup.

The optical and material properties of the encapsulated films were investigated to better understand their behavior. Figure 2a shows the visual aspect of the films (from light blue to light purple) after deposition of the three metal oxides. Changes in color generally indicate a de-doping effect, from oxidized to neutral chains.[52] The UV-Vis-NIR spectroscopy results for the different systems, displayed in Figure 2b, show large variations in absorbance. For the ZnO and Al_2O_3 systems in particular, the broad feature that appears between 700 and 1200 nm indicates the presence of less oxidized PEDOT chains,[53] which must be an effect of metal oxide deposition. Furthermore, all the coated samples have higher absorption than bare PEDOT:OTf in the blue/violet visible region (wavelengths below 500 nm), while in in the visible-infrared region,

the absorbance of the coated films is more variable and generally lower than that of bare PEDOT:OTf.

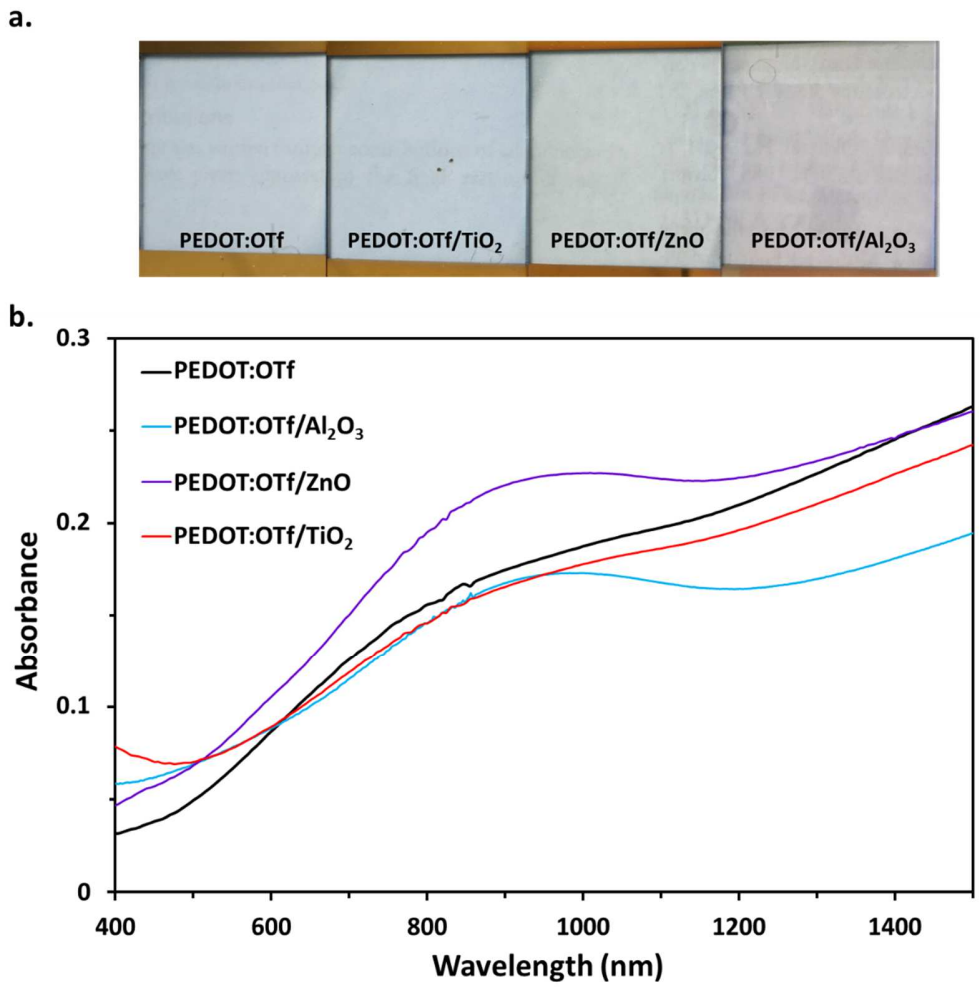

Figure 2. (a) Photographs of bare PEDOT:OTf and PEDOT:OTf encapsulated with Al_2O_3, ZnO or TiO_2 layers, on a glass substrate. (b) Absorbance spectra of PEDOT:OTf thin films encapsulated with Al_2O_3, ZnO and TiO_2 layers.

In order to further understand the individual effect of the oxide layers on the PEDOT:OTf, we performed soft- and hard-XPS (respectively S-XPS and HAXPES) measurements. The chemical impact of the Al_2O_3, ZnO and TiO_2 deposited films was studied through the variation of sulfonate/thiophene ratio (extracted from S2p S-XPS spectra) within the PEDOT:OTf film, with respect to a reference bare sample (Figure 3a-d). The attribution and corresponding fits of the different sulfur doublet peaks in the $S2p_{3/2\text{-}1/2}$ spectra (163.5 - 164.7 eV for thiophene; 168.0 - 169.2 eV for sulfonate) were taken from Gueye et al.[54] In S1s spectra (from HAXPES measurements) the peak at 2470.9 eV was assigned to thiophene groups and the peak at 2477.5 eV to sulfonate groups. The main difference between S-XPS and HAXPES is that the penetration depth with HAXPES is much greater. The penetration depth in XPS varies with the photoelectron mean free path (λ) and take-off angle (θ, here 45°) as $3\lambda \cdot \sin\theta$. The mean free path can be estimated using the Tanuma, Powell and Penn TPP2M formula implemented in the QUASES-IMFP-TPP2M software.[55,56] For S-XPS the estimated penetration depths, based on the inelastic electron mean free path of S2p electron are ~6.6, 5.3 and 5.4 nm for respectively Al_2O_3, ZnO and TiO_2 encapsulation layers. For HAXPES, the estimation of the penetration depth of S1s signal is 12.4, 9.9 and 10.3 nm depth, for Al_2O_3, ZnO and TiO_2 respectively.

The strong increases observed in the sulfonate/thiophene ratio (by S-XPS), from 0.28 without oxide to 0.55 with Al_2O_3 and 0.44 with ZnO (Figure 3a–c), for samples coated with a thin layer (1–2 nm thick, two SALD cycles) to be able to probe the PEDOT:OTf layer, show that Al_2O_3 and ZnO are highly damaging for PEDOT:OTf. For PEDOT:OTf/TiO_2 (Figure 3d) the same effect was observed, but the sulfonate/thiophene ratio only increased to 0.36. Depth profiling of the PEDOT:OTf/TiO_2 sample, using gas cluster ion beam (GCIB) etching, revealed the presence of chloride (from HCl) in the TiO_2 layer (as reported previously[57]) and at the

interface with PEDOT:OTf (Figure 3.e). This is important because it confirms that $TiCl_4$ promotes chloride doping at the interface, potentially increasing the conductivity of the PEDOT:OTf films. In agreement with the conductivity variations observed after oxide deposition, these data indicate that the precursors (DEZ, TMA and $TiCl_4$) react with the PEDOT thin film during SALD. Moreover, the S-XPS measurements performed during abrasion show that the sulfonate/thiophene ratio (i.e. the doping level) of the PEDOT:OTf film decreases with increasing depth (from 0.28 to 0.14 after 8 min of GCIB etching; Figure 3f). Since the conductivity of PEDOT-based materials increases with the level of oxidation,[58] this means that the outer surface (5 nm) of the PEDOT:OTf film is more oxidized than the bulk.

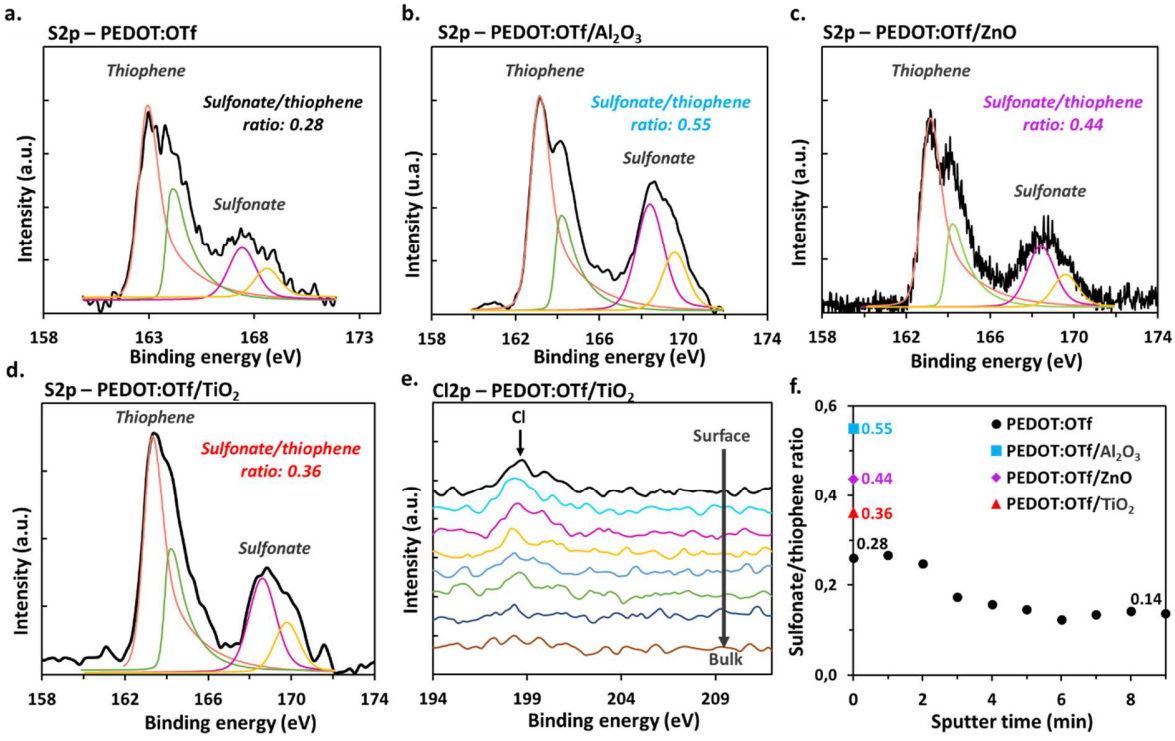

Figure 3. S2p XPS spectra of (a) PEDOT:OTf, (b) PEDOT:OTf/Al_2O_3, (c) PEDOT:OTf/ZnO and (d) PEDOT:OTf/TiO_2, with the corresponding fits. (e) Cl2p XPS spectra of

PEDOT:OTf/TiO_2 at different abrasion times (GCIB; 8 eV/5 nA). (f) Sulfonate/thiophene ratio as a function of the abrasion/sputtering time.

HAXPES measurements (with a greater penetration depth) were also performed on samples treated with 10 cycles of SALD and therefore more representative to the systems used for the aging tests. Figure 4a–d shows the S1s spectra obtained. As expected, the average doping level (sulfonate/thiophene ratio) of the PEDOT:OTf reference sample is lower when calculated from these HAXPES data (0.19 - Figure 4a, representative to the bulk doping) compared to the S-XPS experiment (0.28 - Figure 3a, representative to the outer surface doping). For the PEDOT:OTf/Al_2O_3 film, the increase in the sulfonate/thiophene ratio due to deposition of a thicker oxide layer is less significant (0.44, Figure 4b, versus 0.55, Figure 3b), because Al_2O_3 only damages a few nanometers of the PEDOT:OTf film and acts as a gas barrier thereafter. For the PEDOT:OTf/ZnO sample conversely, the increase in the sulfonate/thiophene ratio is greater after more SALD cycles (0.62, Figure 4c, versus 0.44, Figure 3c). In the case of PEDOT:OTf/TiO_2, the sulfonate/thiophene ratio was measured at 0.28 (Figure 4d) versus 0.36 after just two SALD cycle (Figure 3d), indicating, that the effect of TiO2 deposition is limited to the extreme outer surface of the PEDOT:OTf sample. This is in agreement with the etching results, as shown in Figure 3e.

It is worth noting that the difference between the sulfonate/thiophene ratios measured in the reference PEDOT:OTf sample by S-XPS and HAXPES only reflects the intrinsically different doping levels at the surface and in the bulk of the film. For the encapsulated systems, the variation of sulfonate/thiophene ratio is mainly due to side reactions during oxide deposition that lead to the degradation of the thiophene ring in the PEDOT chains. These results are consistent with the data presented in Figure 1.

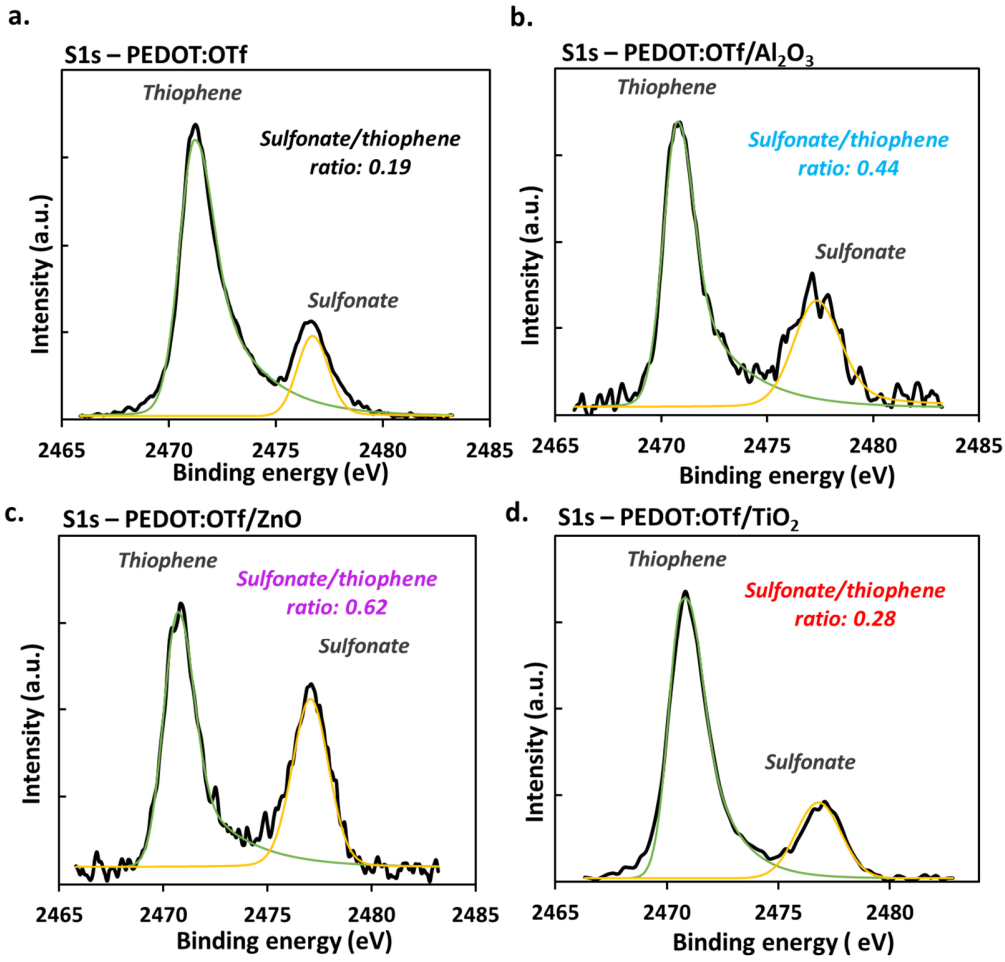

Figure 4. S1s HAXPES spectra of (a) PEDOT:OTf, (b) PEDOT:OTf/Al_2O_3, (c) PEDOT:OTf/ZnO and (d) PEDOT:OTf/TiO_2, with corresponding fits.

Altogether, the results indicate that the only oxide layer that does not increase the resistance of the underlying PEDOT:OTf film during SALD is TiO_2, while only Al_2O_3 and ZnO offer effective encapsulation. Since TiO_2 acts as a gas barrier, we investigated whether it might protect the PEDOT films from the damaging effects of the other metal oxide layers. Bilayer PEDOT:OTf/TiO_2/ZnO and PEDOT:OTf/TiO_2/Al_2O_3 constructs were therefore manufactured and tested as a means to achieve effective protection against solar radiations, without altering the

initial resistance of the underlying film during SALD. Based on previous results, the TiO_2 layer was deposited with 30 cycles (≈20 nm thick) at 150 °C.

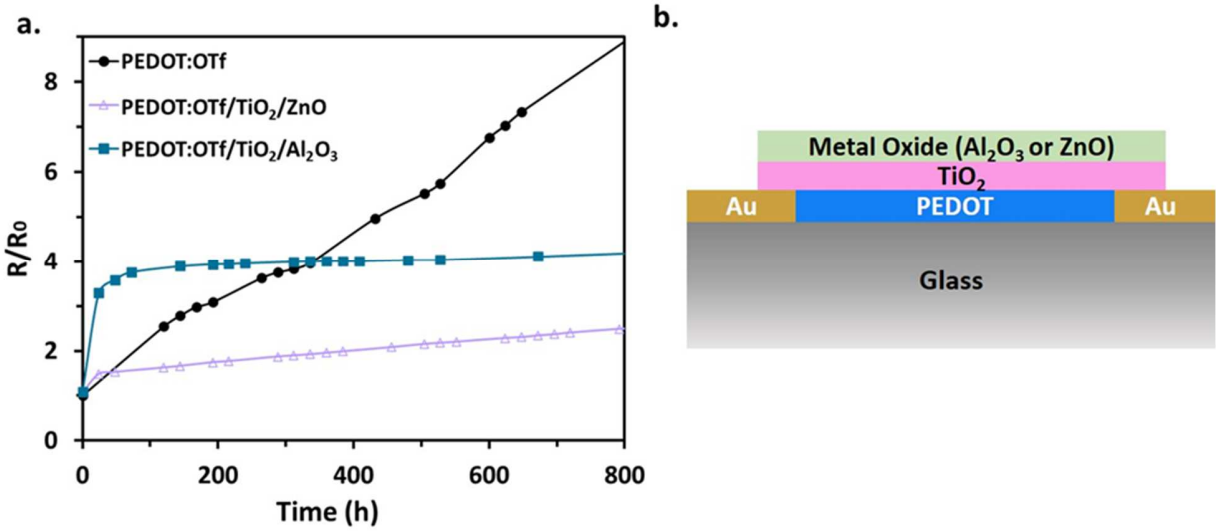

Figure 5. (a) Time evolution of the resistance under 1 sun illumination (1000 W/m²) of PEDOT:OTf encapsulated with bilayers of TiO_2 (30 SALD cycles at 150 °C)/ZnO (20 SALD cycles at 200°C, purple curve) and TiO_2 (30 SALD cycles at 150 °C)/Al_2O_3 (30 SALD cycles at 100°C, blue curve). (b) Schematic representation of the bilayer encapsulated system and experimental setup.

Figure 5a shows that both bilayer architectures (TiO_2/ZnO and TiO_2/Al_2O_3, Figure 5b) provide effective and stable protection under 1 sun illumination, with little increase in resistance either initially or over time. The resistance of the PEDOT:OTf/TiO_2/ZnO sample increased slightly at the very start of the experiments, then increased gradually with a R/R_0 gradient of about 0.0013 h^{-1} and an overall increase of just 2.5-fold over 800 h of sun radiations (compared with a 9-fold increase for the reference film), using the best conditions for ZnO (20 SALD cycles

at 200 °C, see Figure S3 for a list of all deposition conditions). For PEDOT:OTf/TiO_2/Al_2O_3 in contrast, the resistance increased sharply in the first 24 h, before leveling off and remaining virtually constant (R/R_0 gradient of about 0.0006 h^{-1}) for the rest of the experiments. In summary, TiO_2/ZnO encapsulation leads to practically no initial change in the resistance, but the increase over time is about twice as fast as measured for the TiO_2/Al_2O_3 system.

Figure 6a compares all the systems in terms of R_{stab}/R_0, plotted as a function of the slope ($\frac{\Delta R}{R0}*\frac{1}{\Delta t}$), with the stabilized resistance (R_{stab}) being the value at the point where the resistance profile becomes linear. R_{stab} and the slope should ideally be as low as possible. A simple figure of merit (FoM) was calculated from the inverse of the product of these two parameters ($\frac{1}{\text{Slope}*\frac{Rstab}{R0}}$). This FoM has the dimension of a time (h) and corresponds to the delay required for the ratio $R(t)/R_0$ to reach the value $\frac{Rstab}{R0}+\frac{R0}{Rstab}$, with a higher FoM corresponding to better protected system. When there is no initial degradation, the value $\frac{Rstab}{R0}+\frac{R0}{Rstab}$ is equal to 2 (because $R_0 = R_{stab}$) and the FOM corresponds then to the time to double the resistance R_0. Different FoM curves are represented in Figure 6 as dotted lines. The FoM of the non-encapsulated sample is 100 (see Figure 6b), which means that the resistance doubles in just 100 h, compared with 500 h for the TiO_2/Zn system. Looking directly at the scatter plot of FoM values for the different systems (Figure 6a), it is clear that several systems provide effective sun protection. The two bilayer encapsulations offer comparable levels of protection and are on the same FoM line, but not in the same part of FoM space. The pink rectangle in Figure 6a corresponds to samples with extremely low degradation rates ($\Delta R/R_0$*1h sun-aging) but potentially high initial degradation

(R_{stab}/R_0), while the horizontal part (blue rectangle) corresponds to a assemblies with moderate stability and almost no initial degradation.

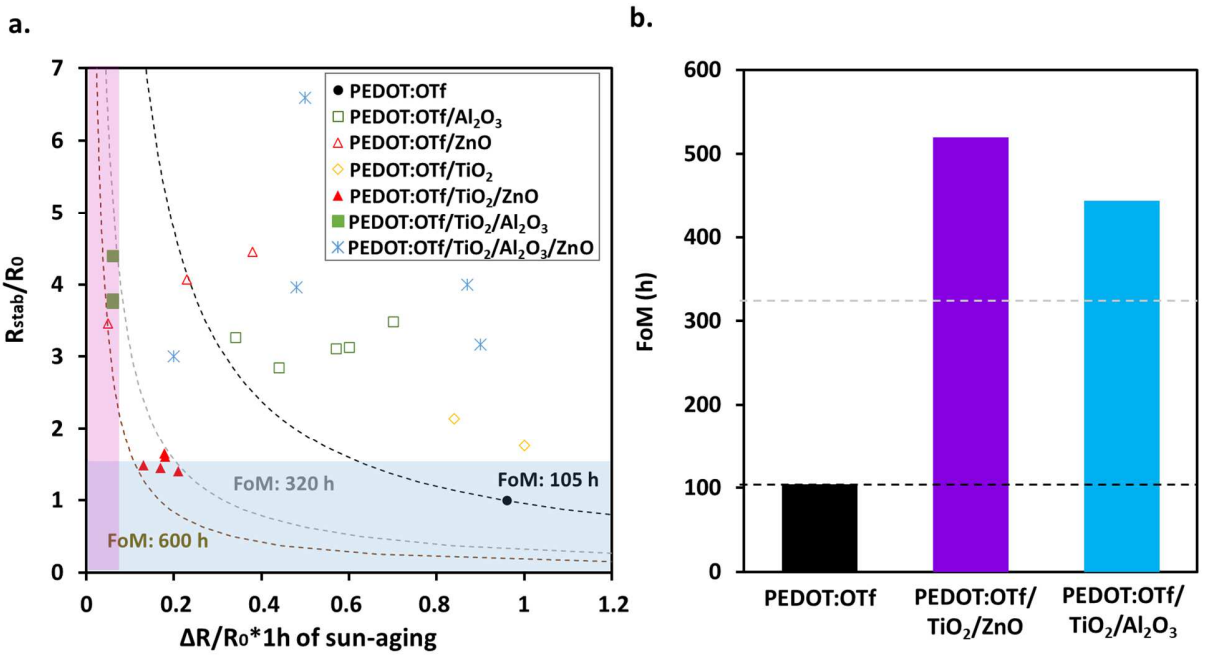

Figure 6. Comparative protective performance under 1 sun illumination of bare PEDOT:OTf (reference), and PEDOT:OTf with monolayer (Al_2O_3, ZnO and TiO_2), bilayer (TiO_2/Al_2O_3 and TiO_2/ZnO) or trilayer (TiO_2/Al_2O_3/ZnO) oxide protection (for different deposition temperatures, from 50°C to 200°C). (a) R_{stab}/R_0 (y-axis) corresponds to the initial non-linear increase in resistance (due to oxide deposition and the first few hours of illumination) before the resistance profile levels off, while $\Delta R/R_0$*1h sun-aging (x-axis) corresponds to the equilibrium rate of increase of the resistance. The dotted lines correspond to different figure of merit values (FoM = (R_{stab}/R_0)*slope). The pink rectangle corresponds to systems with low degradation rates. The blue rectangle corresponds to systems with low initial degradation. (b) Figures or merit for three of the

systems evaluated in the study: PEDOT:OTf (reference without encapsulation), PEDOT:OTf + TiO_2/ZnO and PEDOT:OTf + TiO_2/Al_2O_3.

Trilayer protection with TiO_2, Al_2O_3, and ZnO was tested to see whether the benefits of TiO_2/Al_2O_3 and TiO_2/ZnO — low initial degradation and extremely high stability — could be combined, but the resulting protective effect was inferior to that of the two component bilayers (Figure S4). The likely explanation is delamination, which was visible on the surface of the samples, probably due to interface problems, as is classically observed for multilayer systems.[59–61] Further optimization would be required for this system.

The bilayer TiO_2/ZnO coating, with little initial degradation and good UV protection, was also tested on other PEDOT films having different counter-anions: PEDOT:PSS-EG and PEDOT:Sulf (Figure S5a,b). The results for PEDOT:PSS-EG are similar to those described above for PEDOT:OTf, with deposition leading to a small amount of degradation and the slope of the resistance profile under solar illumination divided by 6 compared with the unprotected film. For PEDOT:Sulf in contrast, although the equilibrium rate of degradation under UV radiation was lower than measured for the bare sample, this did not compensate for the strong initial degradation ($R/R_0 < 4.5$). This difference in behavior compared with the other PEDOT films might be due to the surface reactivity of the already highly doped PEDOT:Sulf with the $TiCl_4$ precursor (used to deposit TiO_2). These results show that to optimize their protective effect, metal oxide coatings have to be adapted specifically to the chemistry of the underlying polymer film.

4. CONCLUSION

This work demonstrates the potential of metal oxides deposited using Spatial Atomic Layer Deposition, an ambient atmosphere and low-cost technique, as UV protective layers for organic PEDOT-based films. Bilayer TiO_2/ZnO and TiO_2/Al_2O_3 protections are shown for the first time here to substantially decrease the degradation rate of the underlying film, while limiting deposition related damage. The combination of TiO_2 and ZnO was found to be particularly effective for both PEDOT:OTf and PEDOT:PSS. XPS and UV-Vis-NIR measurements show that the precursors for ZnO and Al_2O_3 react strongly with PEDOT materials, with a negative effect on their electrical performance. The decrease in the sulfonate/thiophene ratio measured by XPS suggests these reactions probably lead to PEDOT degradation. In contrast, the TiO_2 precursor has a doping effect on the PEDOT films (due to the HCl formed during deposition) and enhances their conductivity. Overall, this work proves that SALD of metal oxides is an efficient method to preserve the electrical performance of conductive polymers used in optoelectronic applications. Novel bilayer structures (TiO_2/ZnO and TiO_2/Al_2O_3) were found to offer the most effective protection and may also be of interest for many other organic materials.

ACKNOWLEDGEMENT

REFERENCES

[1] T.K. Das, S. Prusty, Review on Conducting Polymers and Their Applications, Polym. - Plast. Technol. Eng. 51 (2012) 1487–1500. https://doi.org/10.1080/03602559.2012.710697.

[2] R. Balint, N.J. Cassidy, S.H. Cartmell, Conductive polymers: Towards a smart biomaterial for tissue engineering, Acta Biomater. 10 (2014) 2341–2353. https://doi.org/10.1016/j.actbio.2014.02.015.

[3] C. Zhan, G. Yu, Y. Lu, L. Wang, E. Wujcik, S. Wei, Conductive polymer nanocomposites: a critical review of modern advanced devices, J. Mater. Chem. C. 5 (2017) 1569–1585. https://doi.org/10.1039/c6tc04269d.

[4] T. Nezakati, A. Seifalian, A. Tan, A.M. Seifalian, Conductive Polymers: Opportunities and Challenges in Biomedical Applications, Chem. Rev. 118 (2018) 6766–6843. https://doi.org/10.1021/acs.chemrev.6b00275.

[5] X. Fan, W. Nie, H. Tsai, N. Wang, H. Huang, Y. Cheng, R. Wen, L. Ma, F. Yan, Y. Xia, PEDOT:PSS for Flexible and Stretchable Electronics: Modifications, Strategies, and Applications, Adv. Sci. (2019) 1900813. https://doi.org/10.1002/advs.201900813.

[6] J. Ouyang, Recent Advances of Intrinsically Conductive Polymers, Acta Phys.-Chim. Sinca. 34 (2018) 1211–1220.

[7] S.H. Eom, S. Senthilarasu, P. Uthirakumar, S.C. Yoon, J. Lim, C. Lee, H.S. Lim, J. Lee, S.-H. Lee, Polymer solar cells based on inkjet-printed PEDOT:PSS layer, Org. Electron. 10 (2009) 536–542. https://doi.org/10.1016/j.orgel.2009.01.015.

[8] W. Lu, C. Wang, W. Yue, L. Chen, Si/PEDOT:PSS core/shell nanowire arrays for efficient hybrid solar cells, Nanoscale. 3 (2011) 3631–3634. https://doi.org/10.1039/C1NR10629E.

[9] J.P. Thomas, L. Zhao, D. McGillivray, K.T. Leung, High-efficiency hybrid solar cells by nanostructural modification in PEDOT:PSS with co-solvent addition, J. Mater. Chem. A. 2 (2014) 2383–2389. https://doi.org/10.1039/C3TA14590E.

[10] J.P. Thomas, K.T. Leung, Defect-Minimized PEDOT:PSS/Planar-Si Solar Cell with Very High Efficiency, Adv. Funct. Mater. 24 (2014) 4978–4985. https://doi.org/10.1002/adfm.201400380.

[11] H. Jin, C. Tao, M. Velusamy, M. Aljada, Y. Zhang, M. Hambsch, P.L. Burn, P. Meredith, Efficient, large area ITO-and-PEDOT-free organic solar cell sub-modules, Adv. Mater. Deerfield Beach Fla. 24 (2012) 2572–2577. https://doi.org/10.1002/adma.201104896.

[12] S. Sharma, S. Shriwastava, S. Kumar, K. Bhatt, C.C. Tripathi, Alternative transparent conducting electrode materials for flexible optoelectronic devices, Opto-Electron. Rev. 26 (2018) 223–235. https://doi.org/10.1016/j.opelre.2018.06.004.

[13] E. Yvenou, M. Sandroni, A. Carella, M.N. Gueye, J. Faure-Vincent, S. Pouget, R. Demadrille, J.-P. Simonato, Spray-coated PEDOT:OTf films: thermoelectric properties and integration into a printed thermoelectric generator, Mater. Chem. Front. 4 (2020) 2054–2063. https://doi.org/10.1039/D0QM00265H.

[14] A. Schultheiss, A. Carella, S. Pouget, J. Faure-Vincent, R. Demadrille, A. Revaux, J.-P. Simonato, Water content control during solution-based polymerization: a key to reach extremely high conductivity in PEDOT thin films, J. Mater. Chem. C. (2020) 10.1039.D0TC04899B. https://doi.org/10.1039/D0TC04899B.

[15] A. Schultheiss, A. Revaux, A. Carella, M. Brinkmann, H. Zeng, R. Demadrille, J.-P. Simonato, Electrical and Mechanical Properties of Intrinsically Flexible and Stretchable PEDOT Polymers for

Thermotherapy, ACS Appl. Polym. Mater. (2021) acsapm.1c01203. https://doi.org/10.1021/acsapm.1c01203.
[16] A. Schultheiss, M. Gueye, A. Carella, A. Benayad, S. Pouget, J. Faure-Vincent, R. Demadrille, A. Revaux, J.-P. Simonato, Insight into the Degradation Mechanisms of Highly Conductive Poly(3,4-ethylenedioxythiophene) Thin Films, ACS Appl. Polym. Mater. 2 (2020) 2686–2695. https://doi.org/10.1021/acsapm.0c00301.
[17] N. Chen, X. Wang, K.K. Gleason, Conformal single-layer encapsulation of PEDOT at low substrate temperature, Appl. Surf. Sci. 323 (2014) 2–6. https://doi.org/10.1016/j.apsusc.2014.06.123.
[18] D.H. Levy, D. Freeman, S.F. Nelson, P.J. Cowdery-Corvan, L.M. Irving, Stable ZnO thin film transistors by fast open air atomic layer deposition, Appl. Phys. Lett. 92 (2008) 10–13. https://doi.org/10.1063/1.2924768.
[19] P. Poodt, D.C. Cameron, E. Dickey, S.M. George, V. Kuznetsov, G.N. Parsons, F. Roozeboom, G. Sundaram, A. Vermeer, Spatial atomic layer deposition: A route towards further industrialization of atomic layer deposition, J. Vac. Sci. Technol. Vac. Surf. Films. 30 (2012) 010802. https://doi.org/10.1116/1.3670745.
[20] D. Muñoz-Rojas, J. MacManus-Driscoll, Spatial atmospheric atomic layer deposition: a new laboratory and industrial tool for low-cost photovoltaics, Mater Horiz. 1 (2014) 314–320. https://doi.org/10.1039/C3MH00136A.
[21] D. Muñoz-Rojas, V.H. Nguyen, C. Masse de la Huerta, S. Aghazadehchors, C. Jiménez, D. Bellet, Spatial Atomic Layer Deposition (SALD), an emerging tool for energy materials. Application to new-generation photovoltaic devices and transparent conductive materials, Comptes Rendus Phys. 18 (2017) 391–400. https://doi.org/10.1016/j.crhy.2017.09.004.
[22] C.A.M. de la Huerta, V.H. Nguyen, A. Sekkat, C. Crivello, F. Toldra-Reig, P.B. Veiga, S. Quessada, C. Jimenez, D. Muñoz-Rojas, Gas-Phase 3D Printing of Functional Materials, Adv. Mater. Technol. 5 (2020) 2000657. https://doi.org/10.1002/admt.202000657.
[23] V.H. Nguyen, A. Sekkat, C. Jiménez, D. Muñoz, D. Bellet, D. Muñoz-Rojas, Impact of precursor exposure on process efficiency and film properties in spatial atomic layer deposition, Chem. Eng. J. 403 (2021) 126234. https://doi.org/10.1016/j.cej.2020.126234.
[24] A. Sekkat, V.H. Nguyen, C.A. Masse de La Huerta, L. Rapenne, D. Bellet, A. Kaminski-Cachopo, G. Chichignoud, D. Muñoz-Rojas, Open-air printing of Cu2O thin films with high hole mobility for semitransparent solar harvesters, Commun. Mater. 2 (2021) 1–10. https://doi.org/10.1038/s43246-021-00181-8.
[25] D. won Choi, H. Park, J.H. Lim, T.H. Han, J.S. Park, Three-dimensionally stacked Al2O3/graphene oxide for gas barrier applications, Carbon. 125 (2017) 464–471. https://doi.org/10.1016/j.carbon.2017.09.061.
[26] M.D. Groner, S.M. George, R.S. McLean, P.F. Carcia, Gas diffusion barriers on polymers using Al 2 O 3 atomic layer deposition, Appl. Phys. Lett. 88 (2006) 1–3. https://doi.org/10.1063/1.2168489.
[27] S.L. Schneider, H.W. Lim, A review of inorganic UV filters zinc oxide and titanium dioxide, Photodermatol. Photoimmunol. Photomed. 35 (2019) 442–446. https://doi.org/10.1111/phpp.12439.
[28] T.G. Smijs, S. Pavel, Titanium dioxide and zinc oxide nanoparticles in sunscreens: Focus on their safety and effectiveness, Nanotechnol. Sci. Appl. 4 (2011) 95–112. https://doi.org/10.2147/nsa.s19419.
[29] A. Khan, V.H. Nguyen, D. Muñoz-Rojas, S. Aghazadehchors, C. Jiménez, N.D. Nguyen, D. Bellet, Stability Enhancement of Silver Nanowire Networks with Conformal ZnO Coatings Deposited by Atmospheric Pressure Spatial Atomic Layer Deposition, ACS Appl. Mater. Interfaces. 10 (2018) 19208–19217. https://doi.org/10.1021/acsami.8b03079.

[30] C. Celle, A. Cabos, T. Fontecave, B. Laguitton, A. Benayad, L. Guettaz, N. Pélissier, V.H. Nguyen, D. Bellet, D. Muñoz-Rojas, J.P. Simonato, Oxidation of copper nanowire based transparent electrodes in ambient conditions and their stabilization by encapsulation: Application to transparent film heaters, Nanotechnology. 29 (2018). https://doi.org/10.1088/1361-6528/aaa48e.
[31] K. Ali, K.-H. Choi, J. Jo, Y.W. Lee, High rate roll-to-roll atmospheric atomic layer deposition of Al2O3 thin films towards gas diffusion barriers on polymers, Mater. Lett. 136 (2014) 90–94. https://doi.org/10.1016/j.matlet.2014.07.186.
[32] P.S. Maydannik, T.O. Kääriäinen, K. Lahtinen, D.C. Cameron, M. Söderlund, P. Soininen, P. Johansson, J. Kuusipalo, L. Moro, X. Zeng, Roll-to-roll atomic layer deposition process for flexible electronics encapsulation applications, J. Vac. Sci. Technol. Vac. Surf. Films. 32 (2014) 051603. https://doi.org/10.1116/1.4893428.
[33] Z.P. Ling, Z. Xin, G. Kaur, C. Ke, R. Stangl, Ultra-thin ALD-AlOx/PEDOT:PSS hole selective passivated contacts: An attractive low cost approach to increase solar cell performance, Sol. Energy Mater. Sol. Cells. 185 (2018) 477–486. https://doi.org/10.1016/j.solmat.2018.06.002.
[34] M. Mutee ur Rehman, M. Muqeet Rehman, M. Sajid, J.W. Lee, K.H. Na, J.B. Ko, K.H. Choi, Significance of encapsulating organic temperature sensors through spatial atmospheric atomic layer deposition for protection against humidity, J. Mater. Sci. Mater. Electron. 29 (2018) 14396–14405. https://doi.org/10.1007/s10854-018-9572-4.
[35] P.S. Maydannik, A. Plyushch, M. Sillanpää, D.C. Cameron, Spatial atomic layer deposition: Performance of low temperature H_2O and O_3 oxidant chemistry for flexible electronics encapsulation, J. Vac. Sci. Technol. Vac. Surf. Films. 33 (2015) 031603. https://doi.org/10.1116/1.4914079.
[36] H. Choi, S. Shin, H. Jeon, Y. Choi, J. Kim, S. Kim, S.C. Chung, K. Oh, Fast spatial atomic layer deposition of Al_2O_3 at low temperature (<100 °C) as a gas permeation barrier for flexible organic light-emitting diode displays, J. Vac. Sci. Technol. Vac. Surf. Films. 34 (2016) 01A121. https://doi.org/10.1116/1.4934752.
[37] U. Mehmood, A. Al-Ahmed, I.A. Hussein, Review on recent advances in polythiophene based photovoltaic devices, Renew. Sustain. Energy Rev. 57 (2016) 550–561. https://doi.org/10.1016/j.rser.2015.12.177.
[38] H. Seo, D. Sakamoto, H. Chou, N. Itagaki, K. Koga, M. Shiratani, Progress in photovoltaic performance of organic/inorganic hybrid solar cell based on optimal resistive Si and solvent modified poly(3,4-ethylenedioxythiophene) poly(styrenesulfonate) junction, Prog. Photovolt. Res. Appl. 26 (2018) 145–150. https://doi.org/10.1002/pip.2961.
[39] E. Dauzon, Y. Lin, H. Faber, E. Yengel, X. Sallenave, C. Plesse, F. Goubard, A. Amassian, T.D. Anthopoulos, Stretchable and Transparent Conductive PEDOT:PSS-Based Electrodes for Organic Photovoltaics and Strain Sensors Applications, Adv. Funct. Mater. (2020) 2001251. https://doi.org/10.1002/adfm.202001251.
[40] L. Zhang, K. Yang, R. Chen, Y. Zhou, S. Chen, Y. Zheng, M. Li, C. Xu, X. Tang, Z. Zang, K. Sun, The Role of Mineral Acid Doping of PEDOT:PSS and Its Application in Organic Photovoltaics, Adv. Electron. Mater. 6 (2020) 1900648. https://doi.org/10.1002/aelm.201900648.
[41] A. Schultheiss, M. Gueye, A. Carella, A. Benayad, S. Pouget, J. Faure-Vincent, R. Demadrille, A. Revaux, J.-P. Simonato, Insight into the Degradation Mechanisms of Highly Conductive Poly(3,4-ethylenedioxythiophene) Thin Films, ACS Appl. Polym. Mater. (2020). https://doi.org/10.1021/acsapm.0c00301.
[42] J. Resende, A. Sekkat, V.H. Nguyen, T. Chatin, C. Jiménez, M. Burriel, D. Bellet, D. Muñoz-Rojas, Planar and Transparent Memristive Devices Based on Titanium Oxide Coated Silver Nanowire Networks with Tunable Switching Voltage, Small. (2021) 2007344. https://doi.org/10.1002/smll.202007344.

[43] S. Aghazadehchors, V.H. Nguyen, D. Muñoz-Rojas, C. Jiménez, L. Rapenne, N.D. Nguyen, D. Bellet, Versatility of bilayer metal oxide coatings on silver nanowire networks for enhanced stability with minimal transparency loss, Nanoscale. 11 (2019) 19969–19979. https://doi.org/10.1039/C9NR05658K.
[44] V.H. Nguyen, D. Bellet, B. Masenelli, D. Muñoz-Rojas, Increasing the Electron Mobility of ZnO-Based Transparent Conductive Films Deposited by Open-Air Methods for Enhanced Sensing Performance, ACS Appl. Nano Mater. 1 (2018) 6922–6931. https://doi.org/10.1021/acsanm.8b01745.
[45] M. Juppo, P. Alen, M. Ritala, M. Leskelä, Trimethylaluminum as a reducing agent in the atomic layer deposition of Ti (Al) N thin films, Chem. Vap. Depos. 7 (2001) 211–217.
[46] R.L.Z. Hoye, R.E. Brandt, Y. Ievskaya, S. Heffernan, K.P. Musselman, T. Buonassisi, J.L. MacManus-Driscoll, Perspective: Maintaining surface-phase purity is key to efficient open air fabricated cuprous oxide solar cells, APL Mater. 3 (2015) 020901. https://doi.org/10.1063/1.4913442.
[47] A. Bedia, F.Z. Bedia, M. Aillerie, N. Maloufi, B. Benyoucef, Morphological and Optical Properties of ZnO Thin Films Prepared by Spray Pyrolysis on Glass Substrates at Various Temperatures for Integration in Solar Cell, Energy Procedia. 74 (2015) 529–538. https://doi.org/10.1016/j.egypro.2015.07.740.
[48] V.H. Nguyen, J. Resende, C. Jiménez, J.L. Deschanvres, P. Carroy, D. Muñoz, D. Bellet, D. Muñoz-Rojas, Deposition of ZnO based thin films by atmospheric pressure spatial atomic layer deposition for application in solar cells, J. Renew. Sustain. Energy. 9 (2017). https://doi.org/10.1063/1.4979822.
[49] X. Fan, B. Xu, S. Liu, C. Cui, J. Wang, F. Yan, Transfer-Printed PEDOT:PSS Electrodes Using Mild Acids for High Conductivity and Improved Stability with Application to Flexible Organic Solar Cells, ACS Appl. Mater. Interfaces. 8 (2016) 14029–14036. https://doi.org/10.1021/acsami.6b01389.
[50] L. Bießmann, N. Saxena, N. Hohn, M.A. Hossain, J.G.C. Veinot, P. Müller-Buschbaum, Highly Conducting, Transparent PEDOT:PSS Polymer Electrodes from Post-Treatment with Weak and Strong Acids, Adv. Electron. Mater. (2019) 1800654. https://doi.org/10.1002/aelm.201800654.
[51] A. Fallahzadeh, J. Saghaei, T. Saghaei, Ultra-smooth poly(3,4-ethylene dioxythiophene):poly(styrene sulfonate) films for flexible indium tin oxide-free organic light-emitting diodes, J. Lumin. 169 (2016) 251–255. https://doi.org/10.1016/j.jlumin.2015.09.021.
[52] N. Massonnet, A. Carella, O. Jaudouin, P. Rannou, G. Laval, C. Celle, J.-P. Simonato, Improvement of the Seebeck coefficient of PEDOT:PSS by chemical reduction combined with a novel method for its transfer using free-standing thin films, J. Mater. Chem. C. 2 (2014) 1278–1283. https://doi.org/10.1039/C3TC31674B.
[53] I. Zozoulenko, A. Singh, S.K. Singh, V. Gueskine, X. Crispin, M. Berggren, Polarons, Bipolarons, And Absorption Spectroscopy of PEDOT, ACS Appl. Polym. Mater. 1 (2019) 83–94. https://doi.org/10.1021/acsapm.8b00061.
[54] M.N. Gueye, A. Carella, N. Massonnet, E. Yvenou, S. Brenet, J. Faure-Vincent, S. Pouget, F. Rieutord, H. Okuno, A. Benayad, R. Demadrille, J.-P. Simonato, Structure and Dopant Engineering in PEDOT Thin Films: Practical Tools for a Dramatic Conductivity Enhancement, Chem. Mater. 28 (2016) 3462–3468. https://doi.org/10.1021/acs.chemmater.6b01035.
[55] S. Tanuma, C.J. Powell, D.R. Penn, Calculations of electron inelastic mean free paths. V. Data for 14 organic compounds over the 50–2000 eV range, Surf. Interface Anal. 21 (1994) 165–176. https://doi.org/10.1002/sia.740210302.
[56] Sven Tougaard, QUASES-IMFP-TPP2M, 2000. http://www.quases.com/products/quases-imfp-tpp2m/.
[57] S. Moitzheim, J.E. Balder, P. Poodt, S. Unnikrishnan, S. De Gendt, P.M. Vereecken, Chlorine Doping of Amorphous TiO2 for Increased Capacity and Faster Li+-Ion Storage, Chem. Mater. 29 (2017) 10007–10018. https://doi.org/10.1021/acs.chemmater.7b03478.

[58] H. Shi, C. Liu, Q. Jiang, J. Xu, Effective Approaches to Improve the Electrical Conductivity of PEDOT:PSS: A Review, Adv. Electron. Mater. 1 (2015) 1500017. https://doi.org/10.1002/aelm.201500017.
[59] J. Hu, P.H. Leo, Defect structures at thin film-substrate interfaces, J. Mech. Phys. Solids. 45 (1997) 637–665.
[60] S. Dwarakanath, P.M. Raj, N. Kondekar, M.D. Losego, R. Tummala, Vapor phase infiltration of aluminum oxide into benzocyclobutene-based polymer dielectrics to increase adhesion strength to thin film metal interconnects, J. Vac. Sci. Technol. A. 38 (2020) 033210. https://doi.org/10.1116/1.5141475.
[61] S. Abedini, C. Dong, I.J. Davies, Mechanisms and control of edge interfacial delamination in a multilayer system containing a functionally graded interlayer, Surf. Coat. Technol. 382 (2020) 125221. https://doi.org/10.1016/j.surfcoat.2019.125221.

Encapsulation by Metal Oxides Nanolayers Deposited by SALD